Vacuum 229 (2024) 113504

Contents lists available at ScienceDirect

Vacuum

journal homepage: www.elsevier.com/locate/vacuum

Investigation of anode diameter and keeper geometry influence on open-end emitter heaterless hollow cathode discharge

Jordan H. Hsieh [a], Yi-Lung Huang [a], Ping-Han Huang [a], Yueh-Heng Li [a,b,*]

[a] Department of Aeronautics and Astronautics, National Cheng Kung University, Tainan, 70101, Taiwan
[b] International Doctoral Degree Program on Energy Engineering, National Cheng Kung University, Tainan, 70101, Taiwan

ARTICLE INFO

Handling Editor: Prof. L.G. Hultman

Keywords:
Cathode
Heaterless
Open-end
Keeper
Anode

ABSTRACT

This study explores the impact of anode diameter, keeper-to-cathode distance, orifice diameter, and keeper thickness on the discharge characteristics of the open-end emitter heaterless hollow cathode. The study finds that the discharge voltage positively correlates with the cathode's keeper orifice diameter, attributed to temperature and plasma drift resistance effects. The discharge voltage at 5 sccm and 4 A condition decreased by 4.9 V when the keeper orifice diameter was reduced by 2 mm. The keeper-to-cathode distance also plays a crucial role; shorter distances result in lower discharge voltage oscillations due to reduced ionization-like instabilities in the cathode plume. At 5 sccm and 4 A, the voltage oscillation decreased by 0.6 V when the keeper-to-cathode distance decreased by 4.8 mm. In high discharge current regimes, a thicker keeper orifice requires a higher voltage to sustain the discharge. At 5 sccm and 3 A, the discharge voltage with a 4.8 mm keeper thickness was marginally higher by 0.2 V compared to a 2 mm thickness, while at 6 A, this difference increased to 3.5 V. The findings offer insights into optimizing open-end emitter heaterless hollow cathode designs and lay the groundwork for future studies on cathode plume characteristics.

1. Introduction

Hollow cathodes serve as a type of gas discharge device with broad applications spanning fusion research, manufacturing, and plasma propulsion [1,2]. They have been integral to electric propulsion since the 1960s [3]. Functioning primarily through thermionic emission, hollow cathodes provide a steady stream of electrons. In contrast to pulsed plasma propulsion [4–7], hollow cathodes find routine use in steady-state plasma thrusters, such as ion thrusters [8–12] and Hall thrusters [13], serving as the electron source required for propellant ionization and ion beam neutralization.

The architecture of a hollow cathode predominantly consists of three integral components: the emitter (also referred to as the insert), the cathode tube, and the keeper. The emitter is commonly fabricated from materials with low work functions, such as lanthanum hexaboride, barium oxide, and C12A7 electride [14]. This choice of material facilitates a sufficient thermionic emission current at temperatures below the melting point of the material and its supporting structure. The emitter is typically designed in a cylindrical geometry to enable the passing of neutral gases like xenon, krypton, argon, and iodine through the insert region [15]. The cathode tube serves as the primary structural element, anchoring the emitter and needing to withstand high thermal loads. Crucially, it also maintains chemical stability at elevated temperatures to prevent adverse reactions with the emitter material, which would increase the work function and consequently lead to cathode failure [16].

The third crucial component of the hollow cathode is the keeper, serving several vital roles within the system. First, the keeper acts as an ignitor for the hollow cathode, initiating plasma discharge between itself and the emitter. In the context of heaterless hollow cathodes, the keeper aids in heating the emitter via this discharge mechanism [17]. Second, it assists in maintaining a stable temperature within the cathode and ensures uninterrupted cathode discharge [16]. Lastly, the keeper provides a protective barrier for the cathode tube and emitter against high-energy ion bombardment from the plume region [18].

Before the operation of a hollow cathode, achieving the working temperature of the emitter is pivotal, and generally, two heating methods are employed. The first method utilizes a heater wire wound around the cathode tube. Heat is generated via ohmic heating by passing a substantial current through the wire [19]. This heat is then radiated and conducted to the cathode tube, indirectly raising the temperature of the emitter. The second method involves heating the emitter and

* Corresponding author. Department of Aeronautics and Astronautics, National Cheng Kung University, Tainan, 70101, Taiwan.
E-mail addresses: yueheng@mail.ncku.edu.tw, yuehheng.li@gmail.com (Y.-H. Li).

https://doi.org/10.1016/j.vacuum.2024.113504
Received 19 February 2024; Received in revised form 22 July 2024; Accepted 24 July 2024
Available online 28 July 2024

cathode tube through glow or arc discharge processes. The design adopted in the current study employs the latter approach.

The ignition process for heaterless hollow cathodes can be broadly classified into two phases: plasma breakdown and heating [20]. During the plasma breakdown phase, plasma breakdown occurs between the keeper and the cathode tube. The primary objective of this phase is to generate plasma sufficient for heating the emitter, which is commonly achieved by flowing a large volume of propellant gas through the hollow cathode in a short period while simultaneously applying a high voltage across the keeper and the cathode to initiate a plasma breakdown [21]. After plasma breakdown, the system transitions to the heating phase. Depending on the current limitations set for the keeper, glow discharge or arc discharge may occur [22]. During this phase, both the cathode tube and the emitter are heated through the plasma bombardment, ultimately elevating the emitter to its working temperature, which is conducive to generating a sufficient thermionic emission current for stable cathode operation.

Owing to the absence of an external heater, heaterless hollow cathodes offer several advantages, the most significant being the elimination of thermal fatigue that commonly afflicts heaters due to repeated thermal cycling [23]. Another advantage of a heaterless design is the reduced time required for cathode ignition [24]. In designs featuring hollow cathodes with external heaters, heating is typically an indirect process. The heater is heated first, and then thermal conduction is mainly relied upon to heat the cathode tube. Consequently, this heating process often takes tens of minutes or even hours to elevate the cathode to the desired operating temperature [25]. In contrast, in heaterless designs, the cathode tube and emitter are directly heated by plasma, thereby reducing the time needed to reach thermionic temperatures. This acceleration in the heating process shortens the cathode warm-up time to a matter of seconds [24].

Most existing research on the influence of keeper geometry on heaterless hollow cathodes primarily focuses on optimizing the keeper geometry to reduce the initial breakdown voltage or to minimize the required gas flow rate [26], commonly known as finding the Paschen minimum [27]. Therefore, this study aims to explore the impact of keeper geometry on the discharge characteristics during the steady-state operation of heaterless hollow cathodes, optimizing cathode design to reduce plasma instabilities in the cathode plume and reduce the high energy ion yields. This study further underscores the impact of cylindrical anode diameter on cathode discharge characteristics, building upon recent research that highlighted the influence of anode geometry and surface roughness on the cathode discharge profile [28,29].

Additionally, research on optimizing keeper design has predominantly been based on hollow cathodes with external heaters [30]. Although the designs are similar, the orifice of a heaterless hollow cathode is typically smaller than that of a hollow cathode with an external heater to achieve initial plasma breakdown within reasonable ranges of keeper voltage and gas flow rate. Consequently, one of the objectives of this study is to elucidate the interplays between anode diameter, keeper geometry, and other parameters and how these factors collectively influence the discharge characteristics of heaterless hollow cathodes.

2. Experimental design

2.1. Heaterless hollow cathode

Hollow cathodes can be broadly categorized based on the heating method and the diameter of the cathode tube orifice. In terms of heating, they can be divided into cathodes with external heaters and heaterless hollow cathodes. Based on the diameter of the cathode tube orifice, they are classified into orificed hollow cathodes and open-end emitter hollow cathodes. The former usually features a smaller cathode tube orifice, while the latter virtually lacks such an orifice, with its opening typically similar in size to the emitter's inner diameter. The orifice diameter influences the heating mechanisms that dominate during the self-heating discharge of the cathode.

Self-heating refers to a self-sustaining thermal mechanism in hollow cathodes that allows the emitter to maintain a thermionic temperature without needing external heating. When operating in self-heating mode, the hollow cathode is primarily heated through plasma bombardment in the insert and orifice regions, including electron and ion bombardment [16].

In open-end emitter hollow cathodes, the absence of an orifice leads to a lower neutral gas density than in orificed hollow cathodes. Under these conditions, ions generated within the insert region traverse the sheath potential and impinge upon the emitter surface, resulting in localized surface heating through ion bombardment. The sheath potential in the insert region of an open-end emitter hollow cathode can be described as [16]:

$$\varnothing_s = \varnothing_{wf} - I_d R + \frac{H}{I_d} + \frac{5}{2} T_{eV}, \tag{1}$$

where $\varnothing_s$ denotes sheath potential, $\varnothing_{wf}$ denotes work function, H denotes total heat lost by the emitter, I_d denotes discharge current, R denotes plasma resistance, and T_{eV} denotes electron temperature. Eq. (1) establishes a correlation between the sheath potential and the electron temperature. Given that the neutral gas density within the insert region of an open-end emitter cathode is typically lower than that in the insert region of an orificed cathode, the electron temperature in the former is generally higher than in the latter [16]. The gas pressure within the hollow cathode affects the plasma density and distribution through collisional interactions [31]. Consequently, an increase in sheath potential within the cathode also enhances the kinetic energy of ion bombardment. Fig. 1 presents the open-end emitter heaterless hollow cathode employed in this study.

Fig. 2 illustrates the cross-sectional view of this open-end emitter heaterless hollow cathode. The cathode uses a press-sintered lanthanum hexaboride emitter with an internal diameter of 3.8 mm, an external diameter of 6.35 mm, and a length of 5 mm. The graphite cathode tube has an orifice diameter of 4 mm and is encased by several layers of molybdenum foil serving as a radiation shield. Positioned behind the emitter is a molybdenum spring designed to increase thermal resistance by reducing the cross-sectional area for heat conduction. A graphite gasket is placed between the molybdenum spring and the emitter to prevent chemical reactions between the two at elevated temperatures. The external diameter of the cathode tube is 10 mm.

The keeper has an internal diameter of 24 mm and contains three components: an alumina insulating tube, a tungsten keeper spring, and a

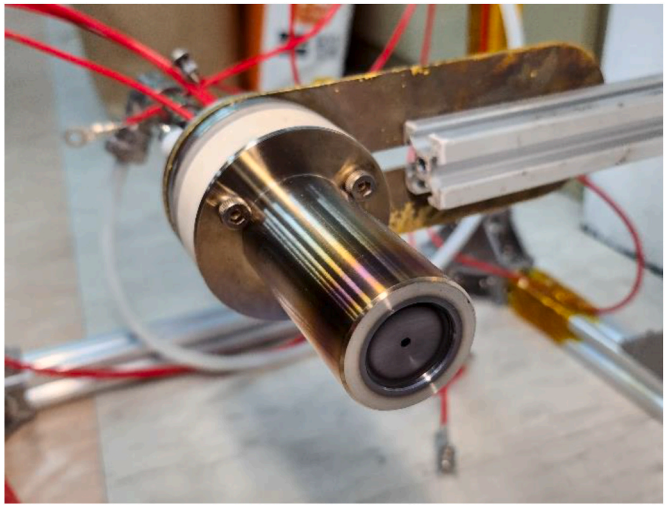

Fig. 1. Photographs of heaterless hollow cathode after 20 h of discharge.

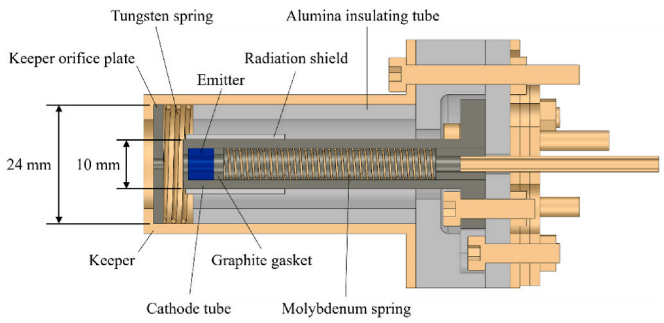

Fig. 2. Cross-section of heaterless hollow cathode.

graphite keeper orifice plate. The alumina insulating tube prevents discharge between the rear end of the cathode tube and the keeper during the ignition phase. The tungsten keeper spring is placed between the alumina insulating tube and the graphite keeper orifice plate, enabling close contact of the keeper orifice plate with the keeper's front end when interchanging orifice plates of different thicknesses. The keeper orifice plate is fabricated from a circular graphite board with a centrally located hole. Due to the cathode design, variables such as the keeper orifice diameter, the thickness of the keeper orifice plate, and the distance from the keeper to the cathode tube can all be adjusted.

2.2. Experimental setup and procedure

The experimental setup employed for this research closely resembles the facilities used in previous studies [25]. The significance of performing stand-alone cathode tests, as conducted in this research, lies in their ability to simulate the operational environment outside a thruster without the influence of a coupling magnetic field [32–34]. This approach is particularly relevant for external-mounted hollow cathodes on Hall thrusters or neutralizer hollow cathodes on ion thrusters, where the external magnetic flux density around these thrusters is typically minimal.

During the experiments, the base pressure of the vacuum chamber was consistently maintained between 10^{-5} Torr to 10^{-4} Torr range. The adopted propellant was 5N2-grade argon with 99.9992 % purity. Electrical measurements capturing the *I–V* envelope of the cathode discharge were carried out using a Teledyne LeCroy HDO4000A oscilloscope with a bandwidth of 1 GHz. The oscilloscope was coupled with two LeCroy PP020 voltage probes, each having a bandwidth of 500 MHz and an input capacitance of 11 pF.

Fig. 3 illustrates the electrical schematics utilized in the current study. During the experiments, the cathode tube, anode power supply, and keeper power supply were all electrically grounded to the common ground of the test facility. The breakdown and sustained discharge between the keeper and the emitter were facilitated by a BK MR100020 DC power supply, capable of providing voltages ranging from 0 to 1000 V and current up to 5 A. The anode-to-emitter discharge was maintained through a BK MR50040 DC power supply, which operates within a voltage range of 0 to 500 V and a current limit of up to 10 A. Voltage probes V_a and V_k were used to measure the anode and keeper potentials, respectively. All electrical connections within the vacuum chamber were established using Teflon-shielded wires to mitigate outgassing interference.

The procedure for heaterless hollow cathode ignition and discharge in this study is delineated as follows:

1) Before each experiment, the cathode was flushed with argon at a flow rate of 40 sccm for 10 min to purge the gas lines.
2) The gas flow rate was then adjusted to 30 sccm, and a voltage of 750 V and a current of 1.2 A were applied to the keeper.

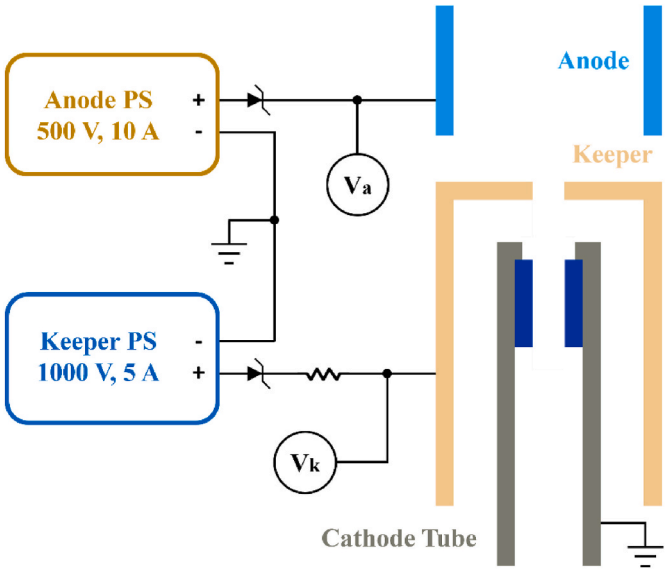

Fig. 3. Electrical circuit for heaterless hollow cathode heating and discharge.

3) After the breakdown occurred between the keeper and the cathode tube, the gas flow rate was reduced to 5 sccm.
4) Upon observing a stable voltage at the keeper, the anode power supply was activated, applying a voltage of 300 V and a current of 3 A.
5) After the anode voltage stabilized, the keeper power supply was deactivated, enabling the cathode to operate in diode mode.

To ensure that the emitter temperature reached thermal equilibrium before data acquisition with the oscilloscope, the cathode was operated under the set flow rate and discharge current conditions for 10 min before each measurement set. If the cathode was exposed to ambient air, a 20-min operational period was initiated before starting the experiment to maintain the condition of the emitter surface.

3. Result and discussion

3.1. Anode diameter influence on discharge voltage

Three cylindrical copper anodes were utilized in this experiment, each measuring 100 mm long, with 102 mm, 74 mm, and 38 mm inner diameter, respectively. These anodes were crafted by rolling 0.1 mm thick copper foils, ensuring consistent surface roughness across all anodes. After the rolling process, each foil cylinder was anchored within two rings made of 2 mm-thick copper. The photographs of the cathode discharges with a 38 mm and a 102 mm anode at a discharge current of 6 A and a flow rate of 6 sccm are shown in Fig. 4. The experimental setup maintained a 6 mm distance between the keeper orifice plate and the cathode tube. The keeper orifice plate had a thickness of 2 mm, and the orifice measured 2 mm in diameter. A gap of 20 mm was maintained between the anode and the keeper tip.

When the cathode is operated with the 102 mm diameter anode in diode mode, maintaining a stable discharge between the cathode and anode proved challenging. Once the primary discharge with anode is established, i.e., the cathode operates in triode mode, turning off the keeper power supply causes the discharge between the emitter and anode to be interrupted and subsequently terminated. A potential explanation for this behavior might be attributed to the momentary shut-off of the keeper power supply, combined with the overly large diameter of the anode and its proximity to the cathode, resulting in a temporary insufficient axial plasma potential to extract enough electrons through the keeper orifice to maintain the primary discharge,

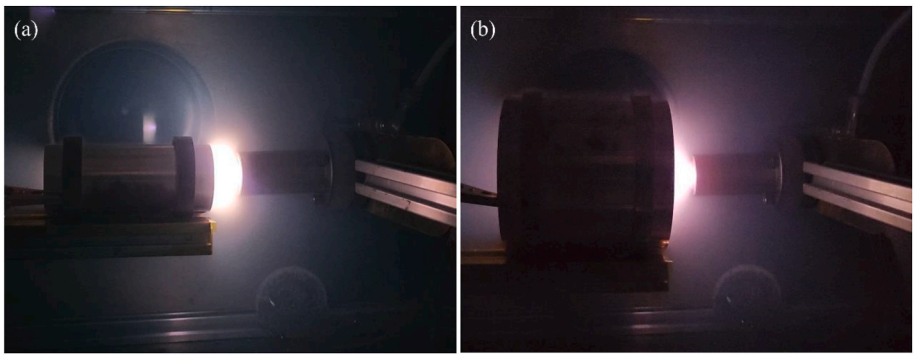

Fig. 4. Photographs of hollow cathode discharge with a (a) 38 mm diameter anode and a (b) 102 mm anode at a discharge current of 6 A and a flow rate of 6 sccm.

leading to the interruption of the discharge.

To address this challenge, when conducting the discharge experiment with the 102 mm diameter anode, the keeper was maintained at a discharge current of 1.2 A, implying its operation in triode mode. In contrast, the keeper was kept floating for the 74 mm and 38 mm anode experiments, in which the cathode is operated in diode mode. Fig. 5 depicts the *I–V* curve of the cathode operation at different discharge currents versus flow rates with different anodes. It is worth noting that the x-axis of the graph represents the total discharge current, which is the sum of the discharge current and the keeper current.

Observations from Fig. 5 delineate three trends concerning the discharge characteristics of an open-end emitter heaterless hollow cathode. Firstly, the discharge voltage of the cathode exhibits an inverse correlation to the discharge current, demonstrating a negative resistance effect. This phenomenon is attributed to reduced emitter sheath voltage [35,36].

Secondly, there is an observed inverse relationship between the steady-state discharge voltage and the gas flow rate. This trend is believed to stem from increased emitter temperature during operation. As the gas flow rate augments, there is a notable increase in the plasma drift resistance [36]. Given that the experiment utilizes an open-end emitter hollow cathode, the drift resistance in the cathode tube orifice remains relatively low across most standard flow regimes. When plasma traverses the keeper orifice, it encounters heightened resistance, leading to an uptick in collisions amongst charged particles. This results in pronounced resistive heating in the orifice plasma. The consequent ohmic power is convectively relayed to the orifice plate through plasma bombardment, which radiatively heats both the cathode tube and emitter [36]. Another factor contributing to the decreased discharge voltage is the increased neutral gas density implied by higher flow rates, which decreases the mean free path of particles and enhances plasma density to a level adequate for the anode power supply [37,38].

Thirdly, the discharge voltage with a 74 mm diameter anode was lower than that with a 38 mm diameter anode; this can be explained by the longer drifting path of electrons in the plume region when the hollow cathode discharges with a larger diameter anode. Fig. 6 depicts the schematic representation of the electron drift paths towards 38 mm and 74 mm anodes. The extended drift path increases the number of ionized neutral particles, reducing the anode voltage necessary to sustain the primary discharge. However, this trend was not observed with the 102

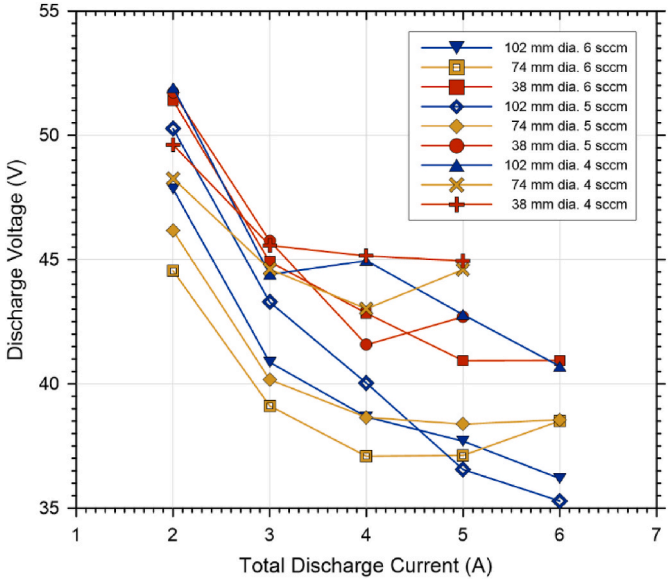

Fig. 5. Plots of the *I–V* curve of cathode discharge with different anodes and operating conditions.

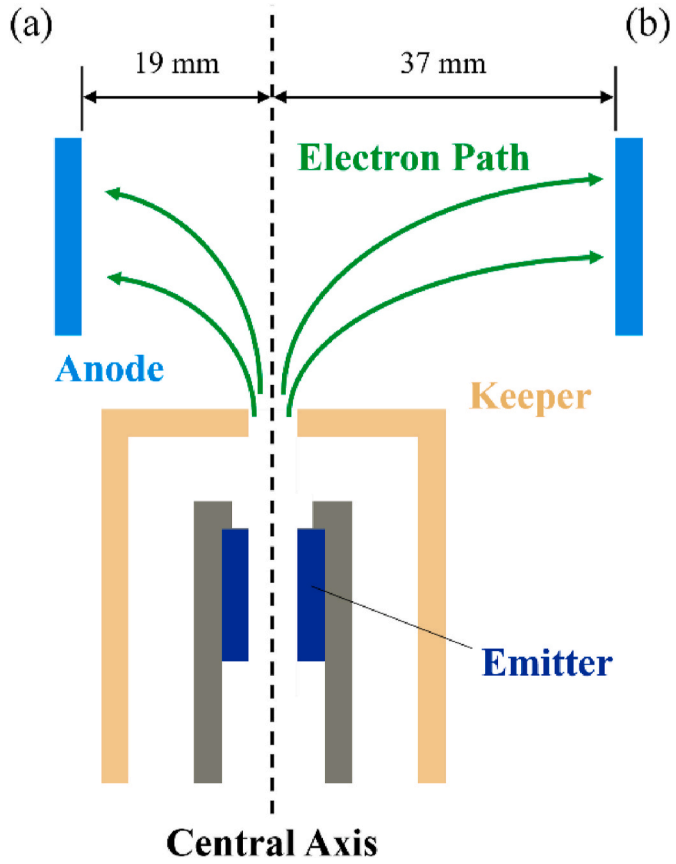

Fig. 6. Electron drift paths toward the (a) 38 mm and (b) 74 mm diameter anodes.

mm anode, presumably because applying a positive bias to the keeper alters its cathode plasma properties compared to operating in diode mode.

3.2. Anode diameter influence on discharge oscillations

The hollow cathode's operational states are often classified into spot and plume modes based on the discharge profile. The spot mode refers to a relatively quiescent and stable discharge mode. In contrast, the plume mode represents a precarious mode where the anode voltage or current typically experiences intense oscillations. The wear on the cathode orifice plate accelerates in plume mode due to the increased production of energetic ions in the plume region [39]. In this study, the definition of the discharge voltage oscillation Δ is as follows:

$$\Delta = \sqrt{\frac{\int_0^{\tau} (V_a - \overline{V}_a)^2 dt}{\tau}}, \tag{2}$$

where τ denotes the measurement time, V_a denotes the discharge voltage, and $\overline{V}_a$ denotes the average discharge voltage. The amplitude in this context was gauged as the standard deviation of the discharge voltage, aligning with methodologies from other studies that evaluate discharge current in Hall thrusters [40]. Fig. 7 illustrates the amplitude of discharge voltage oscillations for the cathode under different operational conditions and with different anodes. The measurement results indicate that the discharge voltage oscillations are lower when the cathode operates with the 38 mm anode than the 74 mm anode; this suggests that in diode mode, a smaller diameter cylindrical anode can more effectively reduce cathode discharge voltage oscillations. It is also observed that as the discharge current increases, the discharge voltage oscillations also intensify at a constant gas flow rate. To further understand the impact of cylindrical anode diameter on cathode discharge characteristics, power spectral density (PSD) analysis is utilized.

Plasma instabilities within the cathode plume exhibit distinct characteristics that allow them to be classified into three types: power supply-induced oscillations, typically below 1 kHz frequency range, ionization-like instabilities occurring within the 10–150 kHz frequency band, and ion-acoustic turbulence (IAT), which manifests at frequencies above 200 kHz [22,39,41]. Recent studies have adopted high-imaging techniques to non-intrusively study the cathode plume, identifying ionization-like instabilities resembling the predator-prey ionization instability often seen in Hall thruster plume [39]. Fig. 8 presents the time-varying waveforms and the PSD analyses for a cathode operating with a 74 mm anode at discharge currents of 6 A and 4 A and a 38 mm anode at 4 A, all at a flow rate of 5 sccm. Fig. 8(a) reveals that the cathode, when discharging at 6 A with the 74 mm anode, experiences the most significant voltage fluctuations, followed by fluctuations at 4 A with the same anode, and the slightest fluctuations occur when discharging at 4 A with the 38 mm anode.

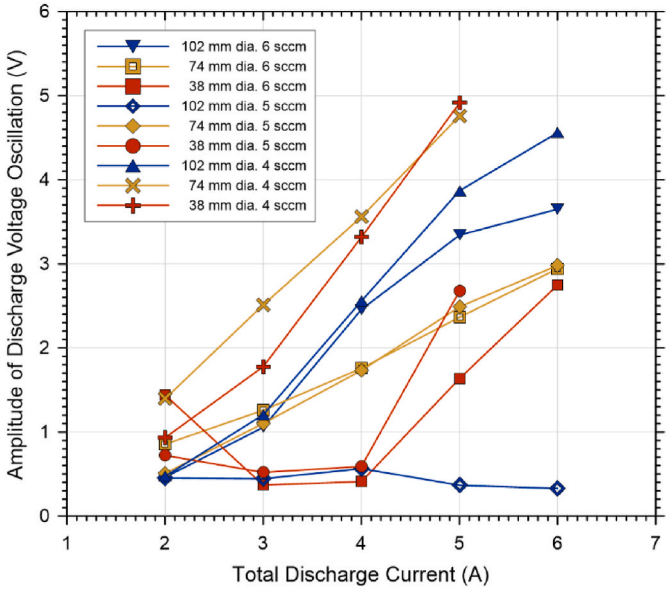

Fig. 7. Plots of the amplitude of discharge voltage oscillation versus the discharge current.

The corresponding PSD analysis in Fig. 8(b) presents a more energetic power spectrum at higher discharge currents with the 74 mm anode, in accordance with the high level of discharge voltage fluctuation observed in Fig. 8(a). The power spectrum also indicates that when the cathode operates at the same gas flow rate and discharge current, a reduction in anode diameter results in a PSD of the discharge voltage similar to that observed with increased gas flow rates or decreased discharge currents. This shift toward a spot mode operation can be attributed to the higher neutral gas density in smaller-diameter cylindrical anodes, where neutral particles are more densely confined within the anode after exiting the keeper orifice. The increased neutral particle density in the plume region quenches ionization-like plume mode instabilities due to a higher collision rate. This elevated collision frequency in the cathode plume also modifies the electron-to-ion temperature ratio and mitigates the IAT growth.

3.3. Keeper orifice influence on discharge characteristics

Three orifice plates of 2 mm thickness were selected in the keeper orifice experiments, each with orifice diameters of 1 mm, 2 mm, and 3 mm, respectively. The distance between the keeper and the cathode tube was 6 mm. The anode fabrication process transitioned from rolled copper film to an integrally formed copper tube for enhanced anode reliability. Given that the hollow cathode in this study has an open-end emitter design (i.e., with a fixed aperture of 3.8 mm for the cathode tube), the internal pressure of the hollow cathode prior to plasma breakdown is primarily determined by the diameter of the keeper orifice. Concurrently, the diameter of the keeper orifice is constrained by the maximum voltage output of the keeper's power supply and the upper limit of the flow rate as indicated by the flow meter. As the diameter of the keeper orifice increases, both the required keeper breakdown voltage and the necessary gas pressure to induce breakdown also rise [26]. The Paschen curve can elucidate this behavior, posing that the pressure between the ignition electrodes dictates the breakdown voltage in a planar electrode configuration, factoring in the inter-electrode distance and electrode materials [27]. Fig. 9 depicts the *I–V* curves and amplitude of discharge voltage oscillations for the cathode fitted with different keeper orifice diameters operating at 6 sccm and 5 sccm gas flows. In subsequent *I–V* curves, the amplitude of discharge voltage oscillation defined in Eq. (2) will be represented using error bars.

The hollow cathode discharge exhibits negative resistance characteristics from Fig. 9, mirroring the prior experiments with anode diameter. Fig. 9(a) shows that when the cathode is subjected to a gas flow rate of 6 sccm in the low discharge current regime, the cathode with a 3 mm diameter keeper orifice presents a relatively higher discharge voltage. However, when the cathode transitions to the high discharge current regime under the same flow rate, the voltage disparity between cathodes with different keeper orifices diminishes. Notably, it was observed during the experiments that when the keeper orifice of the hollow cathode is 1 mm, the cathode cannot sustain a steady-state discharge under conditions of 6 sccm and 6 A. In this configuration, the cathode exhibited significant voltage oscillations and abruptly ceased discharging after 2 to 3 min. Considering the relatively high discharge voltage oscillations observed with a 2 mm orifice compared to a 3 mm orifice at a discharge current of 6 A, it can be explained as particle drift resistance becomes excessively high in the 1 mm orifice under such discharge conditions. This high resistance impedes the effective electron current extraction, leading to the cessation of discharge.

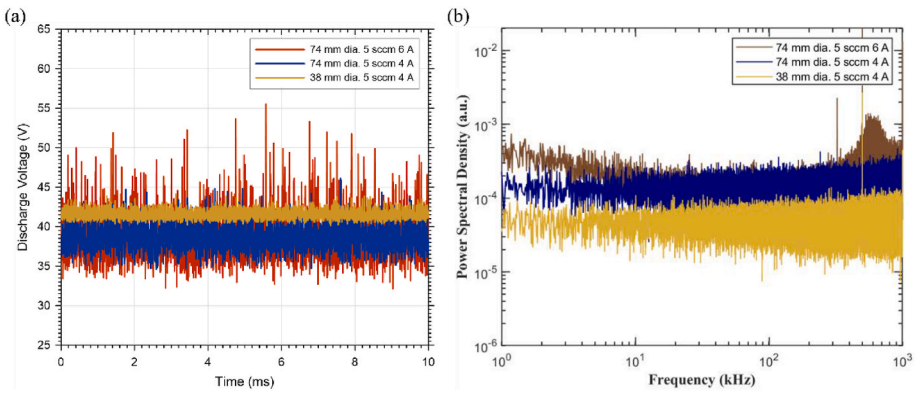

Fig. 8. The (a) time-varying waveforms and (b) power spectral density with the gas flow rate of 5 sccm at different discharge conditions.

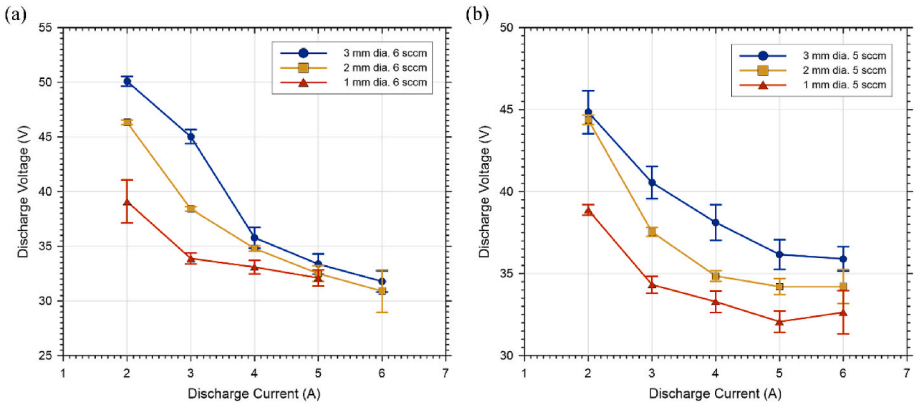

Fig. 9. Plots of the *I–V* curve of the hollow cathode with different keeper orifices at gas flow rates of (a) 6 sccm and (b) 5 sccm.

Another reason for such discharge interruption is the plasma penetration length in the insert region. The plasma attachment length in this region can be decreased by increasing the gas flow rate and discharge current due to the space charge limit [42]. As the flow rate and discharge current increase for a given cathode geometry, the emitter cathode plasma is pushed downstream toward the end of the cathode tube, reducing the plasma contact area with the emitter. In this study, the emitter length is 5 mm, shorter than other hollow cathode designs [22, 42]. Although the shorter emitter was initially chosen to allow the cathode to maintain self-heating at low discharge currents, this design also limits the cathode's performance under high discharge currents and flow rates. When the cathode is discharged with a 1 mm orifice at 6 sccm and 6 A, the plasma in the insert region is excessively pushed downstream, and the space charge limit restricts the thermionic emission current. Additionally, the 5 mm long emitter does not provide a sufficiently long thermionic emission area to sustain enough electron current, resulting in discharge interruption.

A similar trend is also evident in Fig. 9(b). The cathode equipped with a 3 mm diameter keeper orifice consistently exhibits higher discharge voltages at 5 sccm gas flow rates compared to the cathode fitted with 1 mm and 2 mm orifices, while the discharge voltage of 2 mm orifice remains higher than the voltage of 1 mm orifice.

In Fig. 9, there is a noticeable trend that the cathode's discharge voltage is positively correlated to the diameter of the keeper orifice. As this diameter grows, the anode power supply demands a higher voltage to draw enough electrons from the cathode for a consistent control current. On the other hand, a smaller orifice diameter requires less voltage. This behavior is likely tied to the temperature of the keeper orifice plate, which is an outcome attributable to increased plasma resistance R in the keeper orifice [16]:

$$R = \frac{l(\nu_{ei} + \nu_{en})}{\pi r^2 \varepsilon_o \omega_p^2}, \tag{3}$$

where l denotes the orifice length, r denotes the orifice radius, ν_{ei} denotes the electron-ion collision frequency, ν_{en} denotes the electron-neutral collision frequency, ε_o denotes the permittivity of free space, and ω_p denotes the electron plasma frequency. Eq. (3) indicates that plasma resistance in the orifice region is inversely proportional to the square of the orifice's radius. Reducing the keeper orifice diameter enhances plasma drift resistance, raising the keeper orifice plate's temperature. Consequently, this heightened temperature results in a more substantial radiant heat transfer to the cathode tube and emitter, lowering the voltage needed to achieve the desired discharge current for the anode power supply.

Furthermore, it is intuitively evident that the diameter of the keeper orifice impacts the gas pressure within the cathode. Fig. 10 illustrates the variation in argon gas pressure along the cathode's central axis, corresponding to different keeper orifice diameters and gas flow rates. Analytical gas flow equations determine this pressure profile and conform to the modified Poiseuille law, adapted for compressible gases [16]. Elevated gas pressure within the cathode can potentially enhance the ionization rate of neutral particles, leading to increased plasma density. This escalation in plasma density can, in turn, reduce the discharge voltage required for sustaining the cathode operation.

Observations from Fig. 9(a) and (b) suggest that in most discharge current scenarios, the discharge voltage oscillations for cathodes with 1 mm and 3 mm keeper orifices are higher than those with a 2 mm orifice. The PSD analysis of the discharge voltage at a cathode discharge condition of 4 A and 6 sccm, as depicted in Fig. 11, uncovers noteworthy patterns. The analysis indicates that the cathode with a 3 mm keeper

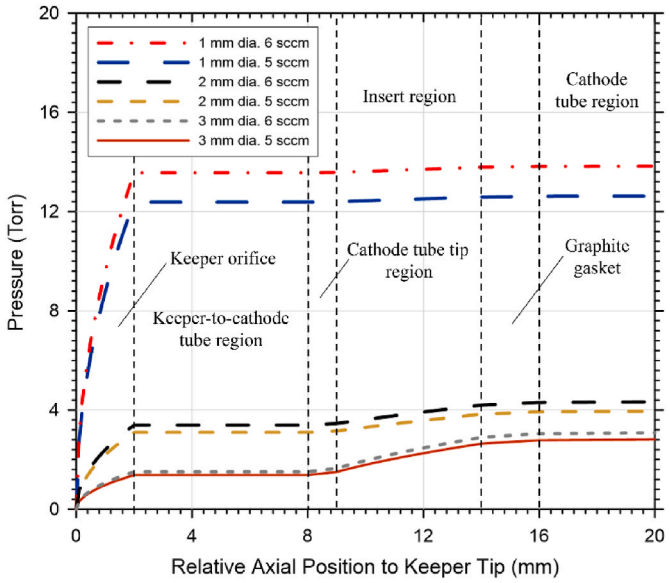

Fig. 10. Neutral gas pressure along the cathode center corresponds to different orifice diameters and flow rates.

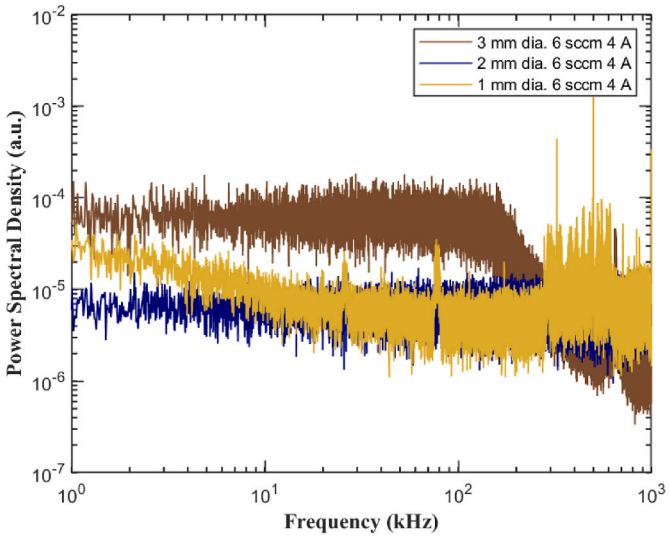

Fig. 11. The power spectral density at the discharge current of 4 A with the gas flow rate of 6 sccm.

orifice exhibits the most energetic spectrum in the frequency domain of approximately 1 to 200 kHz, with a slight peak observed in the range of 500 to 800 kHz. The cathode with a 1 mm keeper orifice displays a strengthened energetic spectrum in the 200 to 1000 kHz frequency range.

The higher discharge voltage oscillation and peak energetic spectrum in the 3 mm keeper orifice cathode can be attributed to the relatively low neutral particle density throughout the cathode. The 3 mm keeper orifice is unable to effectively maintain pressure within the cathode, which increases the mean electron temperature in the insert region and enhances plasma instabilities in the plume region, resulting in a plume mode-like PSD.

The increased discharge voltage oscillation and energetic spectrum observed in the cathode with a 1 mm keeper orifice are related to the limited plasma attachment length and heightened plasma resistance within the keeper orifice. As previously mentioned, the excessive gas flow rate restricts the thermionic emission area downstream toward the cathode tube end. The 1 mm keeper orifice increases the neutral pressure within the cathode, further limiting the plasma attachment length. The limited thermionic emission area causes ionization-like instabilities observed in the PSD analysis. Additionally, the increased plasma resistance at the keeper orifice potentially makes the electron currents passing through the keeper more unstable, thereby amplifying the discharge oscillation.

3.4. *Keeper distance influence on discharge characteristics*

The distance between the keeper orifice plate and the cathode tube tip is adjustable in the cathode design used for this research. This adjustment is made by placing a graphite cylinder of a variable but maximum length of 6 mm between the keeper and the keeper orifice plate. Cross-sectional views for keeper-to-cathode distances of 6 mm and 1.2 mm are shown in Fig. 12.

In most studies that explore heaterless hollow cathode keeper-to-cathode tube distance, the primary focus tends to be understanding its impact on breakdown voltage [24,26]. Specifically, these studies often aim to locate the Paschen minimum by altering this distance. However, this study will focus on how this distance affects the steady-state discharge characteristics of open-end emitter heaterless hollow cathodes.

A tungsten spring positioned between the keeper's interior and the alumina insulating tube serves to press against and secure the keeper orifice plate and the graphite cylinder to the front end of the keeper. The presence of the tungsten spring ensures structural consistency in the

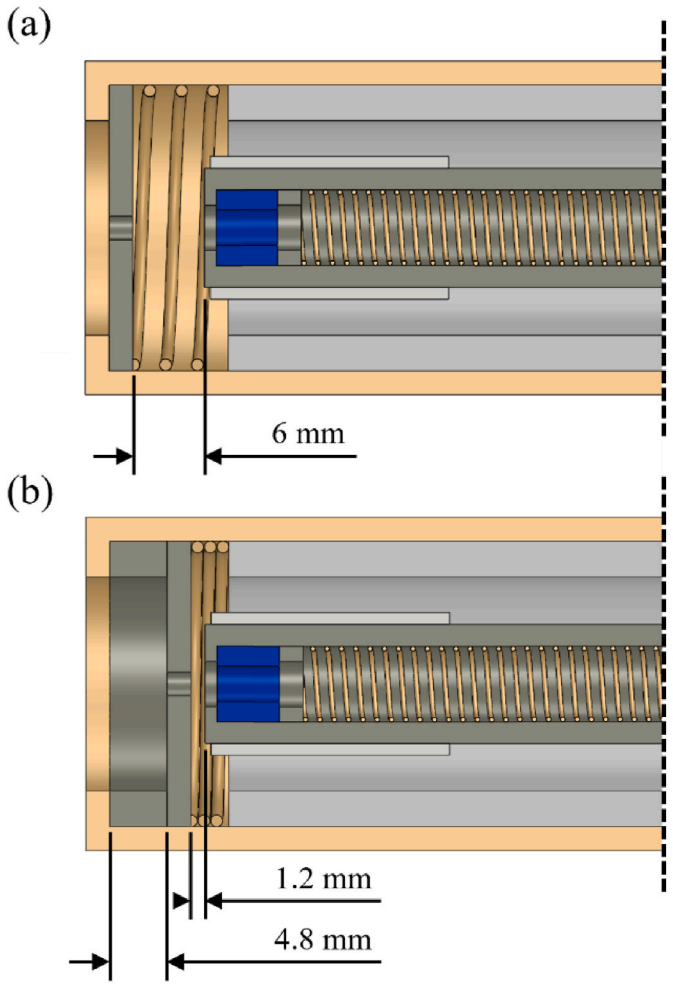

Fig. 12. Cathode configurations for the keeper-to-cathode distance of (a) 6 mm and (b) 1.2 mm.

cathode across different keeper-to-cathode distance configurations, thereby facilitating data comparability in experiments. Three distance variables were considered in these experiments: 6 mm, 3.5 mm, and 1.2 mm. Throughout these tests, the thickness of the keeper's orifice plate remained constant at 2 mm with an orifice diameter of 3 mm. Fig. 13 shows the *I–V* curves and discharge voltage oscillations at these varying keeper-to-cathode distances.

Three key observations emerge from Fig. 13. First, the cathode configuration with a keeper-to-cathode distance of 6 mm exhibits higher discharge voltages than configurations featuring distances of 3.5 mm and 1.2 mm. Second, the configuration with a 1.2 mm distance between the keeper and cathode displays a slightly elevated discharge voltage. Lastly, the configuration with a 1.2 mm keeper-to-cathode distance generally experiences the lowest levels of discharge voltage oscillation, suggesting that this configuration effectively reduces the plasma oscillations in the plume region.

Fig. 14 shows the calculated neutral gas pressure within the cathode corresponding to three keeper-to-cathode distances. In accordance with the gas pressure, it is hypothesized that the slightly higher discharge voltage in the cathode configuration with the 1.2 mm keeper-to-cathode distance, compared to the 3.5 mm distance, can be attributed to the additional space between the keeper and cathode tube in the latter. This extra space allows the accumulation of more argon particles within the keeper's front end. As a result, the cathode with a 3.5 mm keeper-to-cathode distance exhibits a greater argon ionization rate during discharge, reducing the required discharge voltage.

Despite having the most effective neutral particle accumulation, the highest discharge voltage was observed at a keeper-to-cathode distance of 6 mm. This could be attributed to an excessive distance hampering the extraction of the electron current through the keeper orifice, as delineated in Fig. 15. It is worth noting that despite changes in the keeper-to-cathode distance, the anode-to-emitter distance remains the same for all cathode configurations, with the anode-to-keeper tip distance fixed at 20 mm, as shown in Fig. 12. When the keeper-to-cathode distance increases, the inner wall of the keeper gradually becomes an obstacle for the plasma bridge, ultimately raising the required discharge voltage to maintain the primary discharge.

Notably, the represented electron drifting path in Fig. 15 is a simplified schematic; the actual plasma potential varies with the cathode configuration. Concurrently, the 3 mm diameter keeper orifice presents minimal drift resistance for cathode plasma, limiting the heating effect on the cathode tube through radiation from the keeper orifice plate. This phenomenon potentially elucidates why the discharge voltage is not lower in the 1.2 mm keeper-to-cathode distance configuration, where the keeper orifice plate and cathode tube are closer.

Fig. 13 demonstrates a positive correlation between discharge voltage oscillation and keeper-to-cathode distance, mirroring the transition from spot mode to plume mode operation in hollow cathodes.

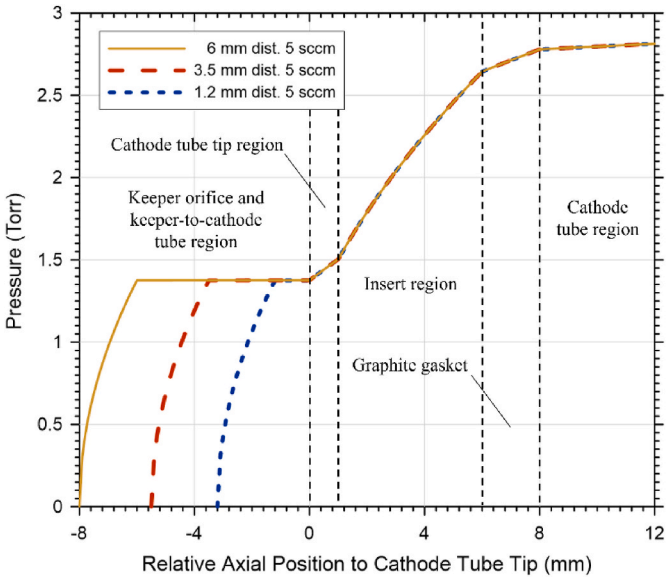

Fig. 14. Neutral gas pressure along the cathode center corresponds to different keeper-to-cathode distances.

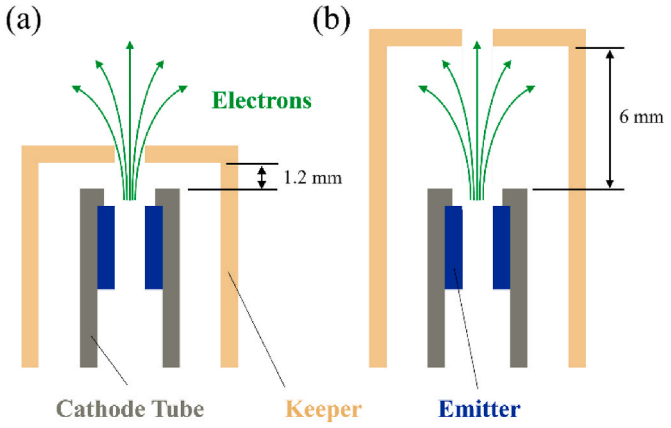

Fig. 15. Electron drifting path with a keeper-to-cathode distance of (a) 1.2 mm and (b) 6 mm.

Plume mode occurs when the gas flow rate falls below a certain threshold or the discharge current exceeds a specific level. Fig. 16 offers a detailed PSD analysis for cathode configurations with keeper-to-cathode distances of 1.2 mm, 3.5 mm, and 6 mm, operating at 4 sccm

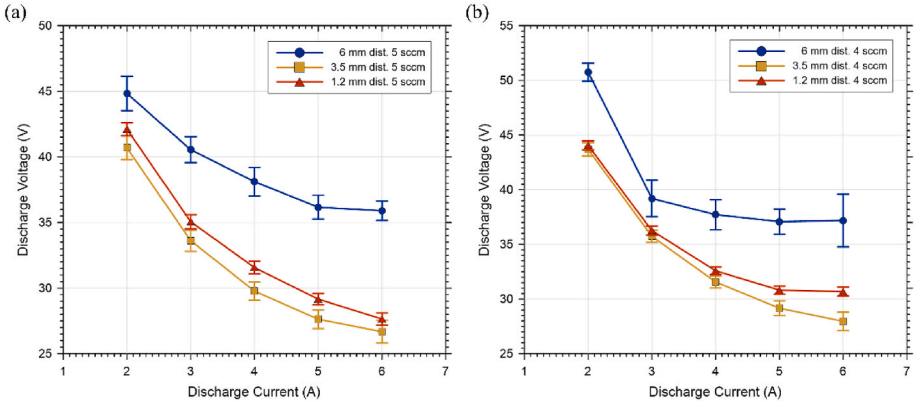

Fig. 13. Plots of the *I–V* curve of the hollow cathode with different keeper-to-cathode distances at gas flow rates of (a) 5 sccm and (b) 4 sccm.

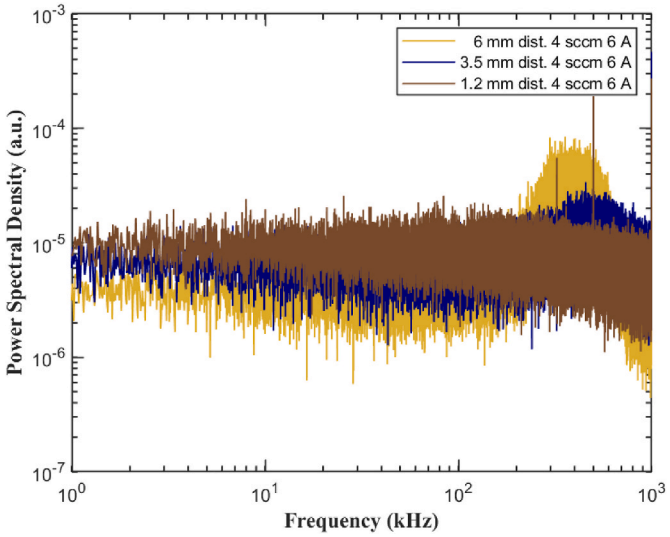

Fig. 16. The power spectral density at the discharge current of 6 A with the gas flow rate of 4 sccm.

and 6 A.

The PSD in Fig. 16 presents a classical spot and plume mode spectrum, despite it being a result of varying keeper-to-cathode distances instead of changing the discharge current or gas flow rate. The correlation between keeper-to-cathode distance and plasma oscillation can be attributed to the distribution and density of neutral particles in the plume region. In configurations with a shorter distance, neutral gas exiting the cathode tube encounters the keeper across a reduced contact area, providing sufficient neutral particles to the plume region to quench ionization-like instabilities. Additionally, the closer proximity of the keeper to the cathode tube allows gas to enter the plume at wider angles relative to the cathode's central axis, resulting in a more evenly spread and extensive neutral gas distribution in the plume region. Consequently, this results in the spot mode-like flat PSD. On the other hand, a larger keeper-to-cathode distance presents a plume mode-like PSD, indicating the enhancement of ionization-like instabilities in the cathode plume region, leading to the production of high-energy ions that can limit the cathode's lifetime.

3.5. Keeper thickness influence on discharge characteristics

The wear and tear of the keeper is one of the typical lifespan-limiting factors for hollow cathodes [43]. During hollow cathode discharge, the keeper is subjected to high-energy ions emanating from the plume region. Over time, these high-energy ions wear out the keeper, exposing the cathode tube and ultimately leading to hollow cathode failure. Therefore, the thickness of the keeper is a crucial factor in determining the lifespan of a hollow cathode. However, an excessively thick keeper can also increase the discharge voltage due to increased plasma resistance. Additionally, the thickness of the keeper orifice affects the density of neutral gas and plasma within the hollow cathode during discharge. For heaterless hollow cathodes, the keeper thickness can also impact the breakdown voltage.

Fig. 17 provides cross-sectional diagrams of cathode configurations with keeper orifice plates of 4.8 mm and 1 mm thickness. Graphite shims are added to the cathode's rear end when installing keeper orifice plates of varying thicknesses to maintain a keeper-to-cathode distance of 1.2 mm. 1 mm, 2 mm, and 4.8 mm are selected as three orifice plate thicknesses to analyze the influence of keeper orifice plate thickness on discharge characteristics. The diameter of the keeper orifice remains at 3 mm, and the length of the graphite cylinder at the keeper's front end is consistent at 4.8 mm. It is worth noting that, despite the constant 20 mm distance between the anode and the keeper tip, the distance between the anode and the emitter marginally increases as the larger thickness of the keeper orifice plate is employed.

To achieve the breakdown voltage within the voltage output limit of the keeper power supply, the cathode with a 1 mm thick keeper orifice plate is supplied with 40 sccm of argon during the breakdown phase, increased from the original 30 sccm. Fig. 18 displays the relationship between discharge voltage and discharge current for varying thicknesses of the orifice plate.

In the low discharge current regime (2 to 3 A), it can be observed from Fig. 18 that the thickness of the keeper orifice plate does not significantly impact the discharge voltage. However, in the high discharge current regime (5 to 6 A), the cathode with a 4.8 mm thick keeper orifice plate exhibits a higher discharge voltage than the cathodes with 1 mm and 2 mm thick keeper orifice plates. Additionally, the negative resistance in this configuration is less pronounced than the other two keeper orifice plate thicknesses.

Eq. (3) in subsection 3.3 also illustrates that the plasma resistance at the orifice is directly proportional to the length of the orifice, i.e., the thickness of the orifice plate, which explains the higher required voltage for 4.8 mm thick keeper orifice plate in high discharge current regime. When operating in the low discharge current regime, the internal cathode plasma density remains low (electron current density less than 42.5 A/cm^2) due to the reduced discharge current, causing minimal influence on the discharge voltage by the keeper orifice plate thickness. Conversely, during high discharge current operations, the density of cathode plasma passing through the keeper orifice becomes more substantial (electron current density more than 56.6 A/cm^2), increasing the frequency of electron-ion and electron-neutral collisions. As a result, the thickness of the keeper orifice plate becomes a significant factor influencing the discharge voltage.

When a 1 mm thick orifice plate is used, the discharge voltage of the cathode is generally higher than that with a 2 mm thick plate. This is due

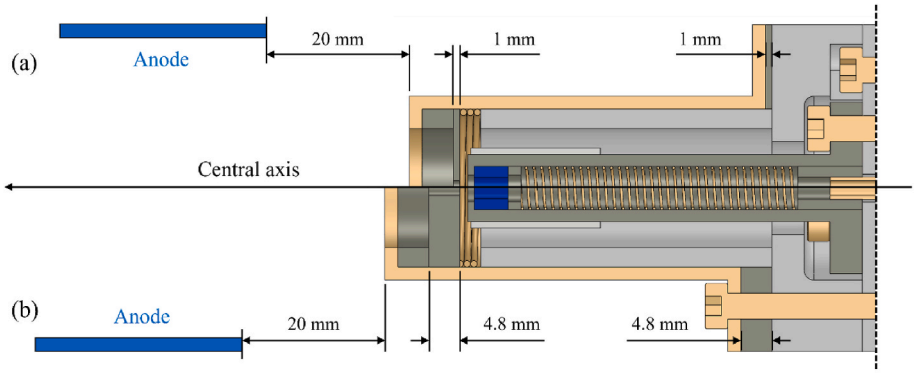

Fig. 17. Cathode configurations for different keeper orifice plate thicknesses of (a) 1 mm and (b) 4.8 mm.

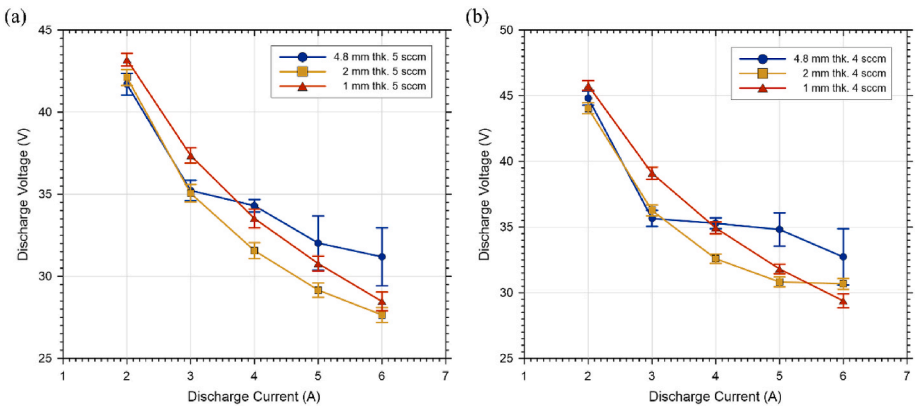

Fig. 18. Plots of the *I–V* curve of the hollow cathode with different keeper orifice plate thicknesses at gas flow rates of (a) 5 sccm and (b) 4 sccm.

to the reduced neutral density within the cathode. Similar to the effect of a shorter keeper-to-cathode distance, the 1 mm keeper thickness cathode fails to maintain internal pressure, leading to a lower density of neutral gas inside the cathode, as supported by Fig. 19, which presents the calculated neutral gas pressure within the cathode corresponding to three keeper orifice plate thicknesses. Although this configuration eliminates plasma penetration issues in the insert region, the lower neutral density decreases the collision frequency and cathode plasma density in the insert region. This, in turn, increases the required discharge voltage to sustain the primary discharge.

Another notable observation from Fig. 18 is the positive correlation between the thickness of the keeper orifice plate and discharge voltage oscillation. This is further substantiated by the PSD analysis shown in Fig. 20, which analyzes three different keeper orifice plate thicknesses operating at 6 sccm and 6 A. The discharge voltage's power spectrum exhibits its highest energy levels with a 4.8 mm thick orifice plate. A marginal increase in the PSD with a 2 mm plate compared to a 1 mm plate hints at a slight enhancement of plasma instabilities in the cathode plume. Notably, no significant peak was observed in the PSD analysis, indicating a spot mode-like PSD. This can be attributed to the sufficient gas flow rate of 6 sccm, which quenches the ionization-like instabilities in the plume region.

The relationship between keeper orifice plate thickness and plasma instabilities in the plume region is thought to be related to the velocity of

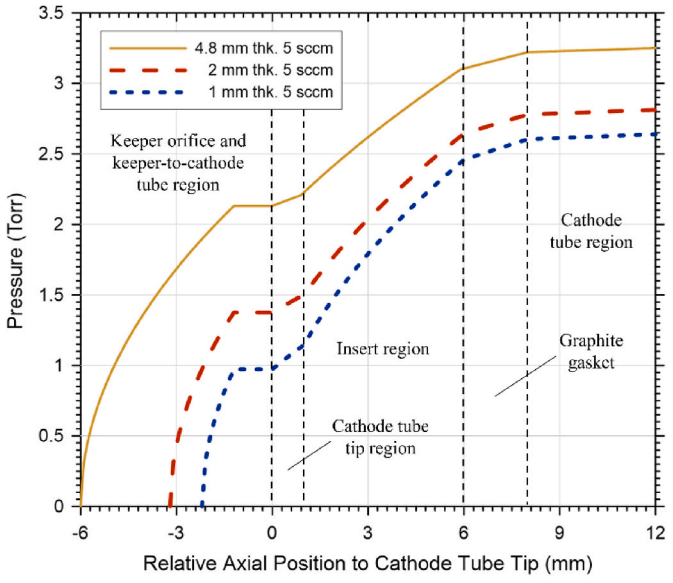

Fig. 19. Neutral gas pressure along the cathode center corresponds to different keeper orifice plate thicknesses.

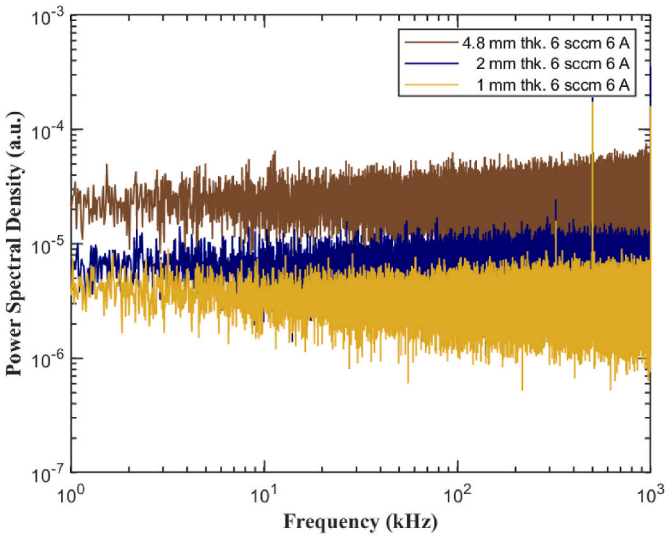

Fig. 20. The power spectral density with different orifice plate thicknesses at the discharge current of 6 A with the gas flow rate of 6 sccm.

argon particles. Under the same orifice diameter conditions, it stands to reason that orifice plate thickness would directly affect the internal neutral gas pressure of the hollow cathode, as presented in Fig. 19. When the cathode has higher internal gas pressure, the neutral particles can drift into the cathode plume region more rapidly due to the high-pressure gradient, reducing the time spent traversing through the cylindrical anode and decreasing the rate of collision. The decreased collision rate leads to increased plasma instabilities. Conversely, with thinner orifice plates, neutral particles enter the cathode plume region with lower velocities, allowing them to remain inside the anode for extended periods and promoting a broader gas distribution, thereby suppressing discharge oscillation.

4. Conclusion

This study investigates the influence of various parameters on the characteristics of an open-end emitter heaterless hollow cathode discharge, including anode diameter, orifice diameter, keeper-to-cathode distance, and keeper orifice plate thickness. These variables shape the discharge properties, influencing aspects such as discharge voltage, plasma drift resistance, and overall stability of the cathode discharge.

In the experiments with various anode diameters, the discharge voltage inversely correlated with anode diameter during diode mode operation, with lower voltage attributed to a longer electron drift path in

the plume region, enhancing neutral particle ionization. Operating in triode mode was essential for stable discharge using the 102 mm diameter anode, as the anode diameter was too large. The power spectral density (PSD) analysis revealed that the higher gas density within the 38 mm diameter anode, the smallest anode, quenches the ionization-like instabilities in the cathode plume, mirroring the plume-to-spot mode transition.

Three orifice diameters (1 mm, 2 mm, and 3 mm) were tested in the experiments on keeper orifice effects in hollow cathodes. The findings demonstrate a direct relationship between orifice diameter and discharge voltage, influenced by plasma resistance and the neutral particle density within the cathode. Notably, the 1 mm keeper orifice cathode fails to maintain discharge at 6 sccm and 6 A due to the insufficient emitter length and space charge limit. The enhanced discharge oscillation observed in the cathode with a 3 mm orifice is caused by the electrons leaving the cathode becoming more energetic due to the low gas pressure. The increased ionization-like instabilities observed in the 1 mm keeper orifice cathode are due to the reduced thermionic emission area of the emitter and increased plasma resistance at the keeper orifice.

Furthermore, the study assessed varying keeper-to-cathode distances, discovering that a 6 mm distance led to higher discharge voltage compared to both 3.5 mm and 1.2 mm configurations. This increased voltage is due to the keeper gradually becoming an obstruction to the plasma bridge as the keeper-to-cathode distance increases, thereby increasing the required discharge voltage. In contrast, the 3.5 mm distance required a lower discharge voltage compared to the 1.2 mm distance due to an enhanced ionization rate at the keeper-to-cathode region. Notably, both discharge voltage oscillation and the intensity of the power spectrum correlated positively with keeper-to-cathode distance, likely due to the higher collision frequency and broader neutral particle distribution in the plume region, which effectively quenches ionization-like instabilities.

Lastly, in high discharge current regimes, the thickness of the keeper orifice plate influences cathode discharge characteristics. It was found that the 4.8 mm thick plate in these regimes leads to higher discharge voltage compared to the 1 mm and 2 mm plates, which is attributed to the increased plasma resistance within the keeper orifice. PSD analysis of discharge voltage revealed that thicker keeper plates elevate cathode plasma instabilities. This can be explained by the acceleration of neutral particle velocity due to the large pressure gradient in thicker keeper plates, which reduces collision rates and slightly intensifies plasma instabilities. This explanation is supported by the calculated neutral pressure within the cathode.

This work explains how anode diameter and keeper geometry influence the heaterless hollow cathode discharge characteristics, with implications for optimizing configurations in various applications. Future work may include the investigation of different keeper geometry influences on cathode plume characteristics, including plasma potential, plasma density, and electron and ion temperature.

CRediT authorship contribution statement

Jordan H. Hsieh: Writing – review & editing, Writing – original draft, Methodology, Investigation, Formal analysis, Data curation, Conceptualization. **Yi-Lung Huang:** Software, Methodology, Investigation, Formal analysis, Data curation. **Ping-Han Huang:** Investigation, Formal analysis, Conceptualization. **Yueh-Heng Li:** Supervision, Resources, Project administration, Methodology, Investigation, Funding acquisition.

Declaration of competing interest

All authors declared that: (i) no support, financial or otherwise, has been received from any organization that may have an interest in the submitted work; and (ii) there are no other relationships or activities that could appear to have influenced the submitted work.

Data availability

Data will be made available on request.

Acknowledgment

Financial support for this work was provided by the National Science and Technology Council under grant numbers NSTC 112-2628-E-006-005-MY3, NSTC 113-2223-E-006-010 and NSTC 112-2218-E-006-015.

References

[1] D. Goebel, A. Forrester, Plasma studies on a hollow cathode, magnetic multipole ion source for neutral beam injection, Rev. Sci. Instrum. 53 (1982) 810–815.
[2] H. Baránková, L. Bardos, Hollow cathode and hybrid plasma processing, Vacuum 80 (2006) 688–692.
[3] V.K. Rawlin, E.V. Pawlik, A Mercury plasma-bridge neutralizer, J. Spacecraft Rockets 5 (1968) 814–820.
[4] Y.-H. Li, J.-Y. Pan, G. Herdrich, Design and demonstration of micro-scale vacuum cathode arc thruster with inductive energy storage circuit, Acta Astronaut. 172 (2020) 33–46.
[5] Y.-H. Li, S. Palagiri, P.-Y. Chang, C. Montag, G. Herdrich, Plasma behavior in a solid-fed pulsed plasma thruster, Journal of Aeronautics, Astronautics and Aviation 51 (2019) 31–42.
[6] Y.-H. Li, K. Dorn, H.-C. Hsieh, T.-C. Kuo, Y.-C. Hsu, Effect of electrode angle on pulsed plasma thruster performance, Journal of Aeronautics, Astronautics and Aviation 53 (2021) 353–367.
[7] Y.-H. Li, C. Royer, Effect of voltage on second-stage electrodes of dual-stage solid propellant pulsed plasma thruster, Vacuum 167 (2019) 103–112.
[8] P.J. Wilbur, V.K. Rawlin, J. Beattie, Ion thruster development trends and status in the United States, J. Propul. Power 14 (1998) 708–715.
[9] Y.-H. Li, T.-Y. Huang, M.M. Shen, Y.-C. Chen, Development of miniature radio frequency ion thruster with inductively coupled plasma source, Journal of Aeronautics, Astronautics and Aviation 55 (2023) 13–28.
[10] Y.-H. Li, Y.-C. Chen, S.-W. Liu, A.R. Aslan, Prediction and optimization of thrust performance from plasma diagnostics in the inductively coupled plasma of an RF ion thruster, Acta Astronautica 208 (2023) 130–141.
[11] A. Shagayda, D. Kravchenko, M. Selivanov, Near-wall conductivity of primary electrons in the discharge chamber of an ion thruster, J. Aeronaut., Astronaut. Aiation 56 (2024) 603–614.
[12] D. Kravchenko, A. Shagayda, M. Selivanov, Comparative numerical research of plasma in ion thruster discharge chambers with different magnetic system types, J. Aeronaut., Astronaut. Aviation 55 (2023) 535–543.
[13] J.-P. Boeuf, Tutorial: physics and modeling of Hall thrusters, J. Appl. Phys. 121 (2017) 011101.
[14] J.H. Hsieh, Y.-H. Li, Review of hollow cathode discharge: exploring advanced design and optimization, Journal of Aeronautics, Astronautics and Aviation 55 (2023) 385–413.
[15] H. Zhiwei, W. Pingyang, N. Zhongxi, Y. Zhanwen, X. Zongqi, Early experimental investigation of the C12A7 hollow cathode fed on iodine, Plasma Sci. Technol. 24 (2022) 074004.
[16] D.M. Goebel, I. Katz, Fundamentals of Electric Propulsion: Ion and Hall Thrusters, John Wiley & Sons, 2008.
[17] D. Lev, L. Appel, Heaterless Hollow Cathode Technology - A Critical Review, 2016.
[18] A. Suzuki, K. Kinefuchi, D. Ichihara, S. Cho, H. Watanabe, K. Kubota, Energetic ion and plasma oscillation measurements during plume mode operation of a hollow cathode, Phys. Plasmas 30 (2023).
[19] M. McDonald, A. Gallimore, D. Goebel, Note: improved heater design for high-temperature hollow cathodes, Rev. Sci. Instrum. 88 (2017) 026104.
[20] V. Vekselman, Y.E. Krasik, S. Gleizer, V.T. Gurovich, A. Warshavsky, L. Rabinovich, Characterization of a heaterless hollow cathode, J. Propul. Power 29 (2013) 475–486.
[21] G. Becatti, R.W. Conversano, D.M. Goebel, Demonstration of 25,000 ignitions on a proto-flight compact heaterless lanthanum hexaboride hollow cathode, Acta Astronaut. 178 (2021) 181–191.
[22] D.R. Lev, I.G. Mikellides, D. Pedrini, D.M. Goebel, B.A. Jorns, M.S. McDonald, Recent progress in research and development of hollow cathodes for electric propulsion, Reviews of Modern Plasma Physics 3 (2019) 1–89.
[23] D.M. Goebel, R.M. Watkins, Compact lanthanum hexaboride hollow cathode, Rev. Sci. Instrum. 81 (2010) 083504.
[24] H. Eichhorn, K. Schoenbach, T. Tessnow, Paschen's law for a hollow cathode discharge, Appl. Phys. Lett. 63 (1993) 2481–2483.
[25] J.H. Hsieh, M.M. Shen, Y.-H. Li, P.-H. Huang, Development of a lanthanum hexaboride hollow cathode for a magnetic octupole thruster, Vacuum 214 (2023) 112146.
[26] A. Daykin-Iliopoulos, S. Gabriel, I. Golosnoy, K. Kubota, I. Funaki, Investigation of Heaterless Hollow Cathode Breakdown, 2015.
[27] F. Paschen, Ueber die zum funkenübergang in luft: wasserstoff und kohlensäure bei verschiedenen drucken erforderliche potentialdifferenz, JA Barth, 1889.
[28] G.-C. Potrivitu, S. Mazouffre, L. Grimaud, R. Joussot, Anode geometry influence on LaB6 cathode discharge characteristics, Phys. Plasmas 26 (2019) 113506.

[29] J.H. Hsieh, P.-H. Huang, Y.-L. Huang, H. Juwantono, Y.-H. Li, Analysis of anode surface roughness influence on heaterless hollow cathode discharge, Phys. Scripta 99 (2024) 035607.
[30] T. Jack, S. Patterson, D. Fearn, The effect of the keeper electrode on hollow cathode discharge characteristics, in: 36th AIAA/ASME/SAE/ASEE Joint Propulsion Conference and Exhibit, 2000, p. 3533.
[31] I.G. Mikellides, I. Katz, D.M. Goebel, J.E. Polk, Hollow cathode theory and experiment. II. A two-dimensional theoretical model of the emitter region, J. Appl. Phys. 98 (2005) 113303.
[32] R. Joussot, L. Grimaud, S. Mazouffre, Examination of a 5 A-class cathode with a LaB6 flat disk emitter in the 2 A–20 A current range, Vacuum 146 (2017) 52–62.
[33] Y. Oshio, K. Kubota, H. Watanabe, S. Cho, Y. Ohkawa, I. Funaki, Experimental investigation of LaB6 hollow cathode with radiative heater, TRANSACTIONS OF THE Japan SOCIETY FOR AERONAUTICAL AND SPACE SCIENCES, Aerospace Technology Japan 17 (2019) 203–210.
[34] G.-C. Potrivitu, R. Joussot, S. Mazouffre, Anode position influence on discharge modes of a LaB6 cathode in diode configuration, Vacuum 151 (2018) 122–132.
[35] A. Riccardo, A. Mariano, D. Pedrini, F. Paganucci, Preliminary characterization of a LaB6 hollow cathode for low-power Hall effect thrusters, in: 33rd International Electric Propulsion Conference, 2013.
[36] D.M. Goebel, I. Katz, Fundamentals of Electric Propulsion: Ion and Hall Thrusters, John Wiley & Sons, 2008.
[37] G.-C. Potrivitu, L. Xu, S. Huang, M. Rohaizat, S. Xu, Discharge mode transition in a Krypton-fed 1 A-class LaB6 cathode for low-power Hall thrusters for small satellites, J. Appl. Phys. 127 (2020) 064501.
[38] M. Mandell, I. Katz, Theory of hollow operation in spot and plume modes, in: 30th Joint Propulsion Conference and Exhibit, 1994, p. 3134.
[39] D.M. Goebel, G. Becatti, I.G. Mikellides, A. Lopez Ortega, Plasma hollow cathodes, J. Appl. Phys. 130 (2021) 050902.
[40] N. Yamamoto, K. Komurasaki, Y. Arakawa, Discharge current oscillation in Hall thrusters, J. Propul. Power 21 (2005) 870–876.
[41] M. Georgin, Ionization Instability of the Hollow Cathode Plume, 2020.
[42] G. Becatti, D.M. Goebel, 500-A LaB6 Hollow cathode for high power electric thrusters, Vacuum 198 (2022) 110895.
[43] A. Sengupta, J. Brophy, J. Anderson, C. Garner, B. Banks, K. Groh, An overview of the results from the 30,000 hr life test of deep space 1 flight spare ion engine, in: 40th AIAA/ASME/SAE/ASEE Joint Propulsion Conference and Exhibit, 2004, p. 3608.